J Mater Sci (2007) 42:6847–6853
DOI 10.1007/s10853-006-1331-x

Thermoelectrical properties and optical third harmonic generation of Gd-doped PbTe

K. Nouneh · K. J. Plucinski · M. Bakasse · I. V. Kityk

Received: 5 October 2006 / Accepted: 28 November 2006 / Published online: 27 April 2007

Abstract We performed the temperature measurements of transport and non-linear optical properties, particularly optical third harmonic generation of PbTe and Gd-doped PbTe to elucidate the effect of the rare earth ion doping on behavior of the thermal conductivity and the third-order non-linear optical susceptibility. The feature of Gd-doped PbTe shows the existence of small values of the low temperature resistivities, ($10^{-6}\Omega$ cm) and a very significant value of mobility $\mu = 1.5^{*}10^{6}\mathrm{cm}^{2}\mathrm{V}^{-1}\mathrm{s}^{-1}$. The thermal conductivity κ decreases with incorporation of the rare earth ion (Gd) in PbTe matrice. The optical third harmonic generation (THG) shows that the great contribution of the phonons observed for PbGdTe compared to the PbTe, enhances the lattice thermal conductivity of network (k_{ph}).

Introduction

The quality of materials for thermoelectric applications [1] is determined by the figure of merit, $\psi\psi^{\psi}\psi\sigma/\kappa$, here S is Seebeck coefficient; σ is electrical conductivity, and κ is thermal conductivity. Higher thermoelectric properties are achieved due to coexistence of high mobilities (for higher σ with reasonable carrier concentrations), higher band masses (to obtain higher values of S), and lower lattice thermal conductivities, $\kappa = \kappa_e + \kappa_l$, which include both electronic and phonon contributions, respectively. The thermoelectric material most often used in today's Peltier coolers is an alloy of bismuth telluride (Bi_2Te_3) is the thermoelectric material of choice for this application, ZT = 0.9 at room temperature, where the main improvement comes from the reduction in lattice thermal conductivity.; this is know as the thermoelectric effect[2]. In addition to bismuth telluride, there are other thermoelectric materials including lead telluride (PbTe), silicon germanium (SiGe), and bismuth-antimony (BiSb) alloys that are used at various operating temperatures.

Diluted Magnetic Semiconductors (DMS), are semiconductor base solid solutions where a part of cations is replaced by transition metals or rare earth ions. All these materials $Pb_{1-x}Gd_xX$ possess the rock-salt structure with (*NaCl-structure*) and an average Gd^{3+} valence are disproportionate to the valence of Pb^{2+} states. The Gd^{3+} impurity levels are believed to form resonant states close to the top of the valence band, pinning the Fermi level and strongly affecting the transport and thermal properties[3, 4]. Indeed, it was shown that in the system with strong disorder the interaction is in favor of delocalization because electrons may help each other to overcome the random potential. This interaction can create a ''soft'' gap in the electron density of states near Fermi level, which is manifested in the anomalous behavior of the thermal properties and nonlinear optics effects. In a disordered semiconductor the dominant electron-phonon mechanism is temperature dependent [4]. In the case of rare-earth

K. Nouneh
Groupe d'Etude des Semiconducteurs, Université Montpellier II, Place Eugène Bataillon, 34095 Montpellier, France

K. J. Plucinski · I. V. Kityk (✉)
Institute of Physics, J. Dlugosz University of Czestochowa, Aleja Aermii Krajowej 13/15, Czestochowa, Poland
e-mail: i.kityk@ajd.czest.pl

K. J. Plucinski
Institute of Electronics, Military University of Technology, Ul. Kaliskiego 2, Warsaw, Poland

M. Bakasse
Faculty of Science, University Chouaib Doukkali, 24000 El Jadida, Morocco

impurities, the energy of electron states depends primarily on the Coulomb interaction between the localized *f*RE etectrons of the solute [5]. However, the weaker coupling between solute and host states may play a crucial role for the valence state of the rare-earth impurities, assuming that energy of the corresponding excited states are low [6].

In the present paper we will perform the complex investigations of the thermoelectrical properties and optical third harmonic generation (THG) of Gd-doped PbTe crystals which are in polycrystalline form.

Experimenta details

Synthesis of samples

The particular components were put in silica glass crucible with conical tip and inner diameter of 12 mm possessing graphitized walls, evacuated up to 10^{-5} Torr, and sealed off. The nominal composition was $Pb_{0.99}Gd_{0.01}$ Te and the total weight of the load was about 50 g. Next the tube was placed in the vertical furnace of 20 mm in diameter and 70 cm length. The ampoule was held during 3 days at temperature 1000 °C for homogenization and after was cooled with a rate of about 20 mm/day. The process was interrupted when the ampoule went out of the furnace reaching the room temperature. It was observed segregation of Gd in the boule the highest Gd content was in the tip of the crystal.

Hall mobility

Hall effect measurements were carried out using the van-der-Pauw configuration (see Fig. 1). Four contacts at the corners of the sample were fixed on the top surface using silver paste. Each bulk sample and the connection leads were firmly fixed in a separate sample holder to avoid mechanical stresses during the measurements. Electrical measurements were done using Lake Shore 7507 Hall-effect measurement systems. To measure the transport resistance, constant current pulses of 100 mA were applied in two directions to the outer probes of the first sample with a current source (Keithley 220) and the voltage drops were measured through the inner probes with a nanovoltmeter (Keithley 2182) and averaged. Voltage-current characteristics also were measured at different temperatures and magnetic fields in the current range 0–100 mA. Hall-effect data were collected using an IEEE computer interface and IDEAS software provided by Lake Shore. The samples were cooled in a closed cycle cryostat (Advanced Research Systems) and the temperature was controlled using Lake Shore 340 temperature controller. At each temperature the data were collected under different magnetic fields up to

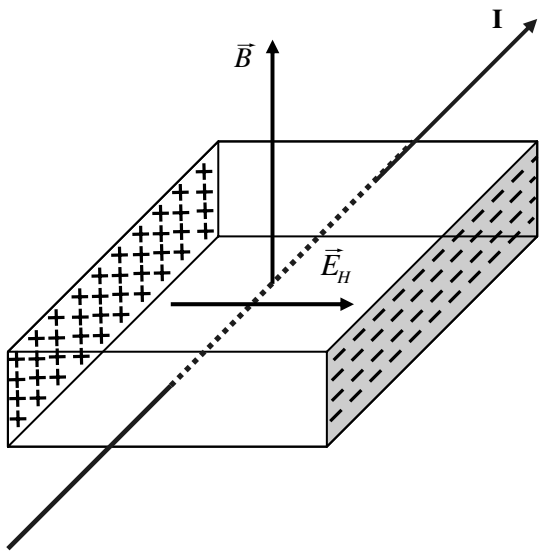

Fig. 1 Principal schema for measurements of van-der-Pauw configuration

1.4 T, using a 7 inch variable gap electromagnet, applied perpendicular to the current direction.

One applies I then one measures V_H, which enables us to determine R_H

$$V_H = \frac{R_H B}{a} I; \tag{1}$$

$R_H = \frac{1}{ne}$, the R_H sign enables us to determine the nature of the charge carriers. Mobility is given by the following relation:

$$\mu = \frac{\sigma}{ne} \tag{2}$$

with $\sigma = 1/\rho, \rho$ is the electrical resistivity.

Transport and thermal properties

During the thermo-power measurements of Seebeck coefficient $S(T)$, we use the hot point method. The basic principle of the method is to create a variation in temperature ΔT in the sample using a hot point and to measure the voltage ΔV that results from the temperature variation. Seebeck coefficient was determined by an expression $S = \Delta V/\Delta T$. The thermal conductivity measurements $\kappa(T)$ between 0.4 K and 300 K were done by a relaxation method using a micro calorimeter and a PPMS apparatus from Quantum Design [7].

THG measurements

We have performed the THG measurements in the reflected geometry using as a fundamental laser beam illumination

of the pulsed Nd-YAG laser with pulse duration 1 ns and pulse rate 10 Hz. Average light power densities were equal to 1.0MW/cm^2 . The sample's temperature was monitored by microthermobolometer chip with accuracy up to 0.3 K. This was done simultaneously from both sides of the samples. The highest observed local heating due to sample absorption did not exceed 0.75 K. Previously it was obtained almost the same value for different investigated photoinduced metals and superconductors [8, 9].

The set-up also allows a monitoring of the specimen's surface by the fundamental light beams. The beam profile sequence had a Gaussian-like shape with a half-width dispersion equal to about 67%. The laser power stability was kept stabilized within 0.1%. The values of the THG coefficients were determined from pump dependences of the reflected tripled frequency signal with respect to the incident ones.

Experimental results

Transport and thermoelectricity properties

From the Fig. 2a and b one can see that in $Pb_{0.099}Gd_{0.01}Te$, the electrical resistivity $\rho(T)$ increases with increasing temperature. In addition we can see in Fig. 2b that the resistivity follows a linear low: $\rho(T) \sim \rho_0 + A^*T$ (1). The remarkably smal values of the low temperature resistivities, $(10^{-6}\Omega\,\mathrm{m})$ in $Pb_{0.099}Gd_{0.01}Te$, can be related to the very high charge carrier mobilities.

Preliminary studies were already carried out by Averous and all [10, 11] on monocrystals of PbGdTe. We present on Fig. 3 the curve of variation of mobility according to the temperature. The mobolity observed is very large and about $4.5.10^6$cm^2/V s and a number of carriers of 2.210^{17}cm^3. These are comparable with the mobilities reported in superlattices.

We also notice that mobility is described by a law $T^{-3/2}$ until 9 K, which indicates that the diffusion is done by the acoustic phonons. Normally at low temperature, the diffusion by the impurities dominant, is characterized by the law in $T^{3/2}$. This behavior are explained by the authors[10, 11], by considering that PbTe has a very large static dielectric constant ε. This great value of ε increases the effect shielding for the Colombian field due to the ionized impurities and the defects so that their effect on displacements of the electrons practically disappear. This can explain the dependence of mobility in $T^{-3/2}$ at low temperature. However the gadolinium atoms behave like donors, when one substitutes them for the lead atoms. And will always take part in the chemical bonds formed with the close atoms. In the case of the combination with PbTe, 2 of the 3 electrons of gadolinium will saturate the layer p with tellurium to form a connection, thus leaving a free electron which takes part in conduction.

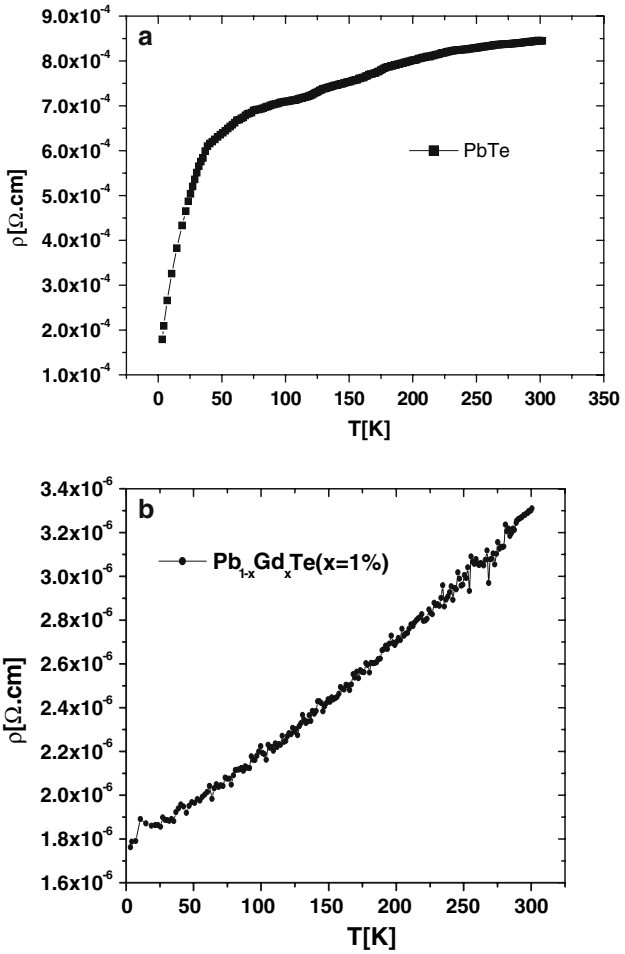

Fig. 2 (**a**) Temperature dependence of the resistivity ρ(T) of PbTe (**b**) Temperature dependence of the resistivity ρ(T) of $Pb_{0.099}Gd_{0.01}Te$

The system of Seebeck measurement is entirely automated and the variations of ΔV according to ΔT are recovered on a plotting table. The line slope obtained

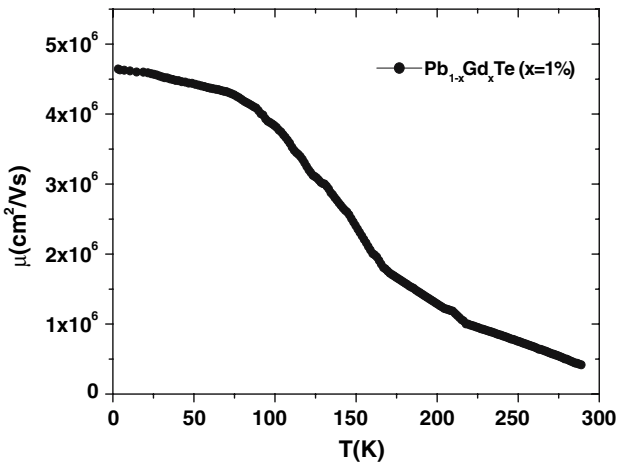

Fig. 3 Hall mobility versus temperature of $Pb_{0.099}Gd_{0.01}Te$

makes it possible to calculate the coefficient of Seebeck via the equation $S = \Delta V/\Delta T$.

In the Fig. 4a and b, are presented the temperature dependence of $\Delta V = f(\Delta T)$ for different samples. This results show that Seebeck coefficient $|S| = 167\mu$V/K and $|S| = 195\mu$V/K for $Pb_{1-x}Gd_xTe$ x=1% and 5% respectively and $|S| = 190\mu$V/K for PbTe are more significant than $Pb_{1-x}Pr_xTe|S| = 60\mu$V/K , the sign negative indicates that we have *n*-type material.

Measurements of thermal conductivity are presented on Fig. 5a and b. The curves show that thermal conductivity varies little in the range of studied temperature. The sample $Pb_{1-x}Gd_xTe$ (x=1%) has a thermal conductivity of about 3.77 W/m K, whereas $Pb_{1-x}Pr_xTe$ (x=1.65%), has a thermal conductivity of a little smaller of about 3.5 W/m.K. It should be mentioned here that these values remain

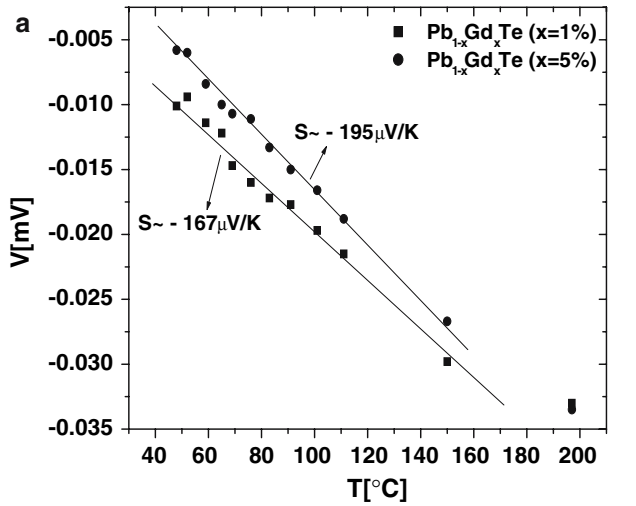

Fig. 4 (**a**) Seebeck coefficient at room temperature of of $Pb_{1-x}Gd_xTe$ (x = 1% and 5%) and $Pb_{1-x}Pr_xTe$ (x = 1.65%) (**b**) Seebeck coefficient at room temperature of of $Pb_{1-x}Pr_xTe$ (x = 1.65% and PbTe

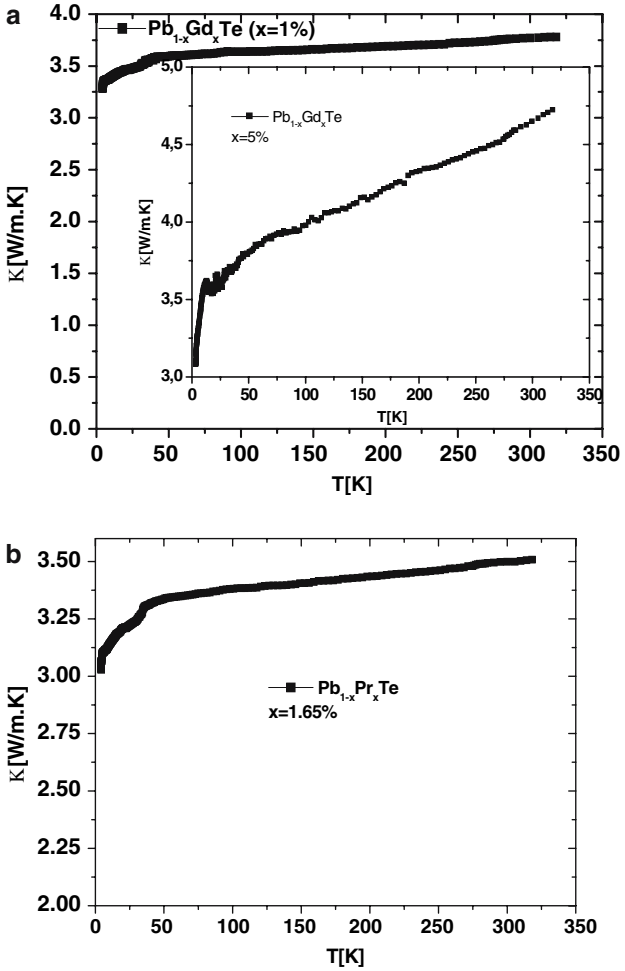

Fig. 5 (**a**) Thermal conductivity versus temperature of $Pb_{1-x}Gd_xTe$ (x = 1–5%) (**b**) Thermal conductivity versus temperature of $Pb_{1-x}Pr_xTe$ (x = 1.65%)

comparable with that of PbTe 3.5 W/m K [12]. These results confirm the observed phenomena in the TPA measurements (see Fig. 6). In the Fig. 6, we can see clearly that the signal of Pr^{3+} is very large than Gd^{3+} , so we have more electron-phonon intercation in PbPrTe compounds compared to the PbGdTe.

Molecular dynamics simulations of microcrystallite sub-system

For describing of the THG we have carried out calculations of the total energy for the investigated materials before and after the illumination by fundamental signal. We have taken into account both electronic and phonon sub-systems

The total energy was calculated using the norm-conserving pseudopotential scheme introduced in the Ref. [13]. The structure of basic molecule was optimized using the quantum chemical package of programs HYPERCHEM-7.5.

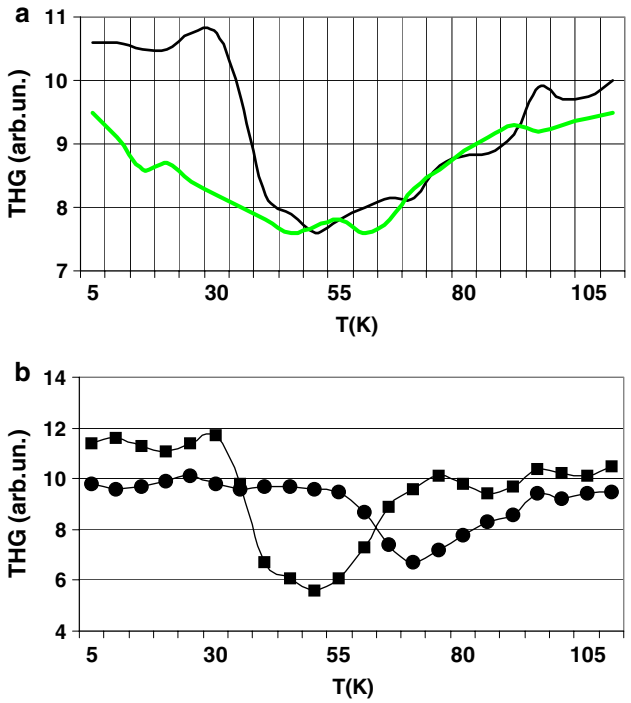

Fig. 6 (**a**) Theoretically calculated temperature dependence of the THG with (dark line) and without (light line) of electron-phonon interaction for $Pb_{1-x}Pr_xTe$ (x = 1.65%) (**b**) Comparison of temperature dependence of TPA in $Pb_{1-x}Gd_xTe$ (x = 1%) (rings), $Pb_{1-x}Pr_xTe$ (x = 1.65%) (squares) and PbTe

The obtained initial wave-functions and atomic positions were used for evaluations of the total energy potentials.

The total energy was expressed within a local density functional approximation with respect to the charge density $\rho(\mathbf{r})$:

$$U[\rho(r)] = T[\rho(\mathbf{r})] + V_{n-e}[\rho(\mathbf{r})] + V_{e-e}[\rho(\mathbf{r})] + V_{e-c}[\rho(\mathbf{r})] \tag{3}$$

where the considered terms correspond to the charge density functionals of the kinetic, nuclear-electron, electron–electron and exchange-electron interactions.

$$\rho(\mathbf{r}) = \Sigma_{\beta,l}|\Psi(l,\mathbf{r},\beta)|^2 \tag{4a}$$

A nonlinear extrapolation procedure was performed to evaluate the fitting coefficients of the corresponding pseudo-wavefunctions, as well as space derivative of pseudopotentials, in a form convenient for analytical evaluations of secular equation's matrix elements, particularly:

$$\Psi(l,\mathbf{r},\beta) = \Sigma_n a_n^{\beta} r^n \exp[-\alpha_n^{(l,\beta)} r^n]$$

where β denotes atom kind, l is the corresponding angular momentum, n determines the level of precision of the nonlinear fitting approach and is varied within the range from 1 to 6. The coefficients a^{β} and $\alpha_n^{(l,\beta)}$ are fitting coefficients evaluated during the nonlinear fitting procedure. The precision of the fit was, better than 0.03 Hartree.

b) *crystalline and quasi-crystalline approaches;*

During the calculations of the non-liner optical properties materials we have done calculations using the structural factors of materials.

The pseudopotential was chosen in a form:

$$V_{ps}^{(\beta,l)} = \Sigma_{i=1}^{3}[A_i^{\beta} + r^2 A_{i+3}^{\beta} \exp(-\alpha_l^{(l,\beta)} r^2)] \tag{5}$$

Here $A_i, A_{i+3}, \alpha_1^{(l,\beta)}$ are fitting coefficients for the ions of β kind and for the MO orbital with angular momentum l. We solved a secular equation corresponding to a pseudopotential written by (5):

$$\begin{aligned}&\|[h^2(\mathbf{K}+\mathbf{G}_n)^2/2m - E(\mathbf{k})]\delta_{n,n'} + \Sigma_\alpha V_\alpha(\mathbf{G}'_n - \mathbf{G}_n)\\ &S_\alpha(\mathbf{G}'_n - \mathbf{G}_n)\| = 0\end{aligned} \tag{6}$$

where $E(\mathbf{k})$is an eigenenergy for a $\mathbf{k}$-point in the MC Brillouin zone, $\mathbf{G}'_n, \mathbf{G}_n$ are wavevectors of interacting plane waves. A structural form-factors for the β-th kind of atoms can be expressed in a form:

$$S_\beta(\mathbf{G}'_n - \mathbf{G}) = g^{(\beta)}/\Omega N_\alpha \Sigma \exp(-l(\mathbf{G}'_n - \mathbf{G}_n)\tau_\beta) \tag{7}$$

Here $g^{(\beta)}$ is a weighting factor determining partial contributions of the disordering to the total potential. Varying the parameter $g^{(\beta)}$ we have operated by the degree of the long-range ordering. The latter factor is particularly important for the interfaces separating particular crystallites and long-range ordering background. Assuming the equilibrium deposition process one can expect that the sizes of the investigated clusters are limited by the occurred interface potential gradients.

Moreover, this approach may be sufficient for different disordered materials and partially ordered solids including the investigated MC. We chose a plane wave basis set consisting of 536–824 plane waves to achieve eigenenergy convergence of about 0.018 eV.

The solution of the secular equation set (Eq. 5) was obtained using a modified Jacobi method QL. Additional (230–268) plane waves from an extended Lowdin basis set were included into the calculations. A Fourier transform of the pseudopotential takes a form:

$$V_\alpha(\mathbf{G}'_n - \mathbf{G}_n) = 1/\Omega \int V_\alpha(\mathbf{r}) \exp[-i(\mathbf{G}'_n - \mathbf{G}_n)r] \tag{8}$$

Electron screening effects were taken into account using a parameterized Perdew-Zunger [9] expression in a form:

$$\mu_{xc} = -0.6193/r_s - 0.14392/(1 + 1.0529r_s^{1/2} + 0.3334r_s)\{1 + [(0.526r_s^{1/2} + 0.3334r_s)/(3(1 + 1.0529r_s^{1/2} + 0.3334r_s))]\} \quad \text{for} \quad r_{s>1} \tag{9}$$

$$\mu_{xc} = -0.6193/r_{s_s} + 0.031\ln(r_s) - 0.0583 \quad \text{for} \quad r_s < 1 \tag{10}$$

where $r_S = [3/(4\pi\rho)]^{1/3}$ with ρ being electron density. The first terms in Eqs. 9 and 10 correspond to a standard Gaspar-Kohn-Sham exchange potential.

Diagonalization procedure was carried out at special weighting points of the BZ for each MC type. Acceleration of the iteration convergence was achieved by transferring 75% of the (m–1)-th iteration result to the m-th iteration. The following condition was taken as a criterion for self-consistency:

$$|(\rho_m - \rho_{m-1})/\rho_m| < \varepsilon \tag{11}$$

We assumed a level of calculation error (ε) better than 0.10%.

The main drawback of all one-electron calculations consists in an underestimation of the band gap values. For this reason self-energy correction renormalization procedure was included in the energy gap calculations.

The effective total potential was built as a superposition of disturbed long-range background and local crystalline contributions:

$$V(\mathbf{G}) = \left(\frac{1}{\Omega_{crc}}\right)_{am^{cr}} \int_{SiC} V^{cr}(\mathbf{r})\exp(-i\mathbf{Gr})d^3\mathbf{r} + \left(\frac{1}{\Omega_{am-grain}}\right) \int_{g_{am-grain}} V^{am-grain}(\mathbf{r})\exp(-i\mathbf{Gr})d^3\mathbf{r} \tag{12}$$

where **G** corresponds to the effective plane-wavevector within the first BZ; g_{am} and g_{cr} correspond to the weighting factors directly connected to concentrations of inter-crystalline interfaces and clusters. V^{am} (**r**) and V^{cr} (**r**) are potentials corresponding to the amorphous-like and crystallite states, respectively.

To accelerate the self-consistent convergence procedure for determining the eigenvalues, we modified the norm-conserving PP wavefunctions through their orthogonalization to the LCAO wavefunctions.

The starting total energy minimization was carried out within the framework of the LDA pseudopotential method. The total energy of the MC film was evaluated as a statistic sum renormalized by an appropriate Boltzmann weighting factor.

To carry out the geometry optimization, we used the molecular dynamics technique described in Ref. [13].

The geometry optimization procedure was started from interfaces between the crystalline and distrubed background. Afterwards we have introduced a varying parameter microcrystallite size **d**. We started from the molecular dynamics interface optimization of the fourth neighboring layers (two from the MC side and two in the direction of the disordered background). About 170–210 atoms from both sides of the interface were taken into account. The molecular dynamics procedure was carried out until the total energy minimum value for a given cluster was the same as for the whole composite. The energy of this composite was determined as a partial sum of the crystallites with a given relative presence of the crystalline interface and polycrystalline phases. At the second stage we considered the next layers of the cluster and repeated the procedure for the new structural geometry. The step-by-step procedure was repeated through an iteration process until the relative displacement of atoms for two successive layers was less than 0.24 Å.

We have found that to achieve a sufficient molecular dynamics geometry convergence, it was necessary to take into account from 6 to 10 such layers depending on the cluster sizes.

Using the described above procedure we determined interface topology significantly varying the geometry of the interface supercluster. The main condition that was used at each step of such molecular base renormalization was similar to the well-known dynamics boundary derivative procedure of Broyden-Fletcher-Goldfarb-Shanoo with variable effective cluster sizes (dynamics boundary conditions) and fulfillment of the condition of total energy minimum conservation.

We also superimposed effective inter-particle dipole-dipole interactions to take into account all the possible quasi-mesoscopic interactions. As a result, we obtained several structural conformations with different values of the total energy minima for a given cluster. In order to establish values of the partial contributions for a given cluster and its neighbors, we introduced weighting factors with values proportional to the probability of their appearance at a given phase. The obtained wave-functions and eigen-energies were used for calculations of the anahrmonic electron-phonon contributions to the non-linear optical susceptibilities as described in the Ref. [14] . In the Fig. 6 a are presented the calculated dependences of the THG for the investigated materials with and without the electron-phonon anharmonicity. One can see that taken into account of electron-phonon anharmonicity give substantially different shape of the THG temperature dependences.

Comparison of the experimental data (Fig. 6b) and of theoretically calculated (Fig. 6a) unambiguously show that

the inclusion of electron-phonon anharmonicity plays a dominant role in the observed effects of the THG, which are sensitive to the phase transformations.

Conclusions

We have established that in $Pb_{0.099}Gd_{0.01}Te$, the electrical resistivity ρ(T) increases with increasing temperature by a linear low: $\rho(T) \sim \rho_0 + A^*T$ (1), and the mobility follows the law: $\mu \infty T^{-3/2}$. Temperature dependences of the Hall effect and thermal; conductivity confirm substantial role of the electron-phononinteractions ion the observed dependences , particularly electron-phonon anharmonicity described by third rank polar tensors and manifested in the non-linear optical effects. The optical dependences of the THG versus temperature unambiguously show a higher sensitivity of the THG compared to the transport properties. This is caused by electron-phonon anharmonicity contribution of the THG, how it was shown from the temperature dependences of the optical susceptibilities.

Acknowledgements We acknowledge helpful discussions with Professor S. Benet (LP2A, University Perpignan, France). S. Charar (Group Etudes Semiconductor GES, University Montpellier II, France) for very useful discussions and suggestions concerning the transport part of the paper and Z. Golacki (Institute of Physics, Warsaw, Poland) for the sample preparations.

References

1. Sales BC, Mandrus D, Chakoumakos BC, Keppens V, Thompson JR (1997) Phys Rev B 56:15081
2. Charar S, Tedenac JC, Potin V, Viennois R, Laire O, Fau C, Liautard B (2000) Physica Status Solidi (A) 182:669
3. Grover B (1965) Phys Rev 140(6A):A 1944
4. Kityk IV, Gruhn W, Sahraoui B (2004) Optics and lasers in engineering 41:51
5. Efros AL, Shklovskii BI (1975) J Phys C: Solid State Phys 8:L49
6. Dugaev VK (2000) Inorg Mater 36(5):524
7. Commercial Apparatus for Measuring Thermal Transport Properties from 1.9 to 390
8. Kityk I (1994) J Phys Condens Matt 6:4119
9. Kityk I, Jakubczyk E (1999) Appl Opt 38:3152
10. Bruno A, Lascaray JP, Averous M, Fillion G, Dumas JF (1988) Phys Rev B 37:1186
11. Averous M, Lombos BA, Fau C, Ilbnouelghazi E, Tedenac JC, Brun G, Bartkowski MA (1985) Phys Stat Sol (b) 131:759
12. Sur I, Casian A, Balandin A (2004) Phy Rev B 69:035306
13. Plucinski K, Kityk IV, Makowska-Janusik M (2000) Cryst Res Technol 3511:1305
14. Tkaczyk S, Kityk IV, Viennois R (2004) . Manifestation of grain boundaries in the transport properties of p-sexiphenyl films.// J Chem Phys (USA), V.121, Is.:517